











## Research Article

# Synthesis and Characterization of New Magnetofluorescent Silicon Dot for Theranostic Application

Nourin Yousefieh <sup>1</sup>, Farinaz Khalatbari <sup>1</sup>, Seyedeh Masoumeh Ghoreishi <sup>2</sup>,  
Mohammad Seyedhamzeh <sup>1</sup>, Farnoor Davachi Omoomi <sup>1</sup>, Mostafa Saffari <sup>3</sup>,  
Sepehr Ashrafi <sup>4,5</sup>, Seyed Esmail Sadat Ebrahimi <sup>6</sup>, Mehdi Mirzaei <sup>7</sup>,  
and Mehdi Shafiee Ardestani <sup>1</sup>

<sup>1</sup>Department of Radiopharmacy, Faculty of Pharmacy, Tehran University of Medical Sciences, Tehran, Iran

<sup>2</sup>Cellular and Molecular Biology Research Center, Health Research Institute, Babol University of Medical Sciences, Babol, Iran

<sup>3</sup>Department of Pharmaceutics & Medical Nanotechnology, Branch of Pharmaceutical Sciences, Islamic Azad University, Tehran, Iran

<sup>4</sup>Department of Pharmaceutics, Faculty of Pharmacy, Tehran University of Medical Sciences, Tehran, Iran

<sup>5</sup>Quality Control Department, Pasteur Institute of Iran, Iran

<sup>6</sup>Department of Medicinal Chemistry, Faculty of Pharmacy, Tehran University of Medical Sciences, Tehran, Iran

<sup>7</sup>Iran Ministry of Health and Medical Education, Deputy Ministry for Education, Tehran, Iran

Correspondence should be addressed to Farinaz Khalatbari; [m.s.hamzeh@gmail.com](mailto:m.s.hamzeh@gmail.com),  
Mohammad Seyedhamzeh; [farina\\_kh@gmail.com](mailto:farina_kh@gmail.com), Mostafa Saffari; [mostafasaffari@gmail.com](mailto:mostafasaffari@gmail.com),  
and Mehdi Shafiee Ardestani; [shafieeardestani@gmail.com](mailto:shafieeardestani@gmail.com)

Received 7 February 2021; Revised 21 January 2022; Accepted 21 February 2022; Published 27 April 2022

Academic Editor: Raul Arenal

Copyright © 2022 Nourin Yousefieh et al. This is an open access article distributed under the Creative Commons Attribution License, which permits unrestricted use, distribution, and reproduction in any medium, provided the original work is properly cited.

**Introduction.** Breast cancer is the leading cause of mortality for women, and effort is being made to provide an agent which has both imaging and therapeutic effects (theranostics) which can improve the survival, economic burden, and outcomes. **Methods.** In this research, for the first time, we introduce a new magnetophotoluminescent quantum dot (Mn-Si-QD) capable of DOX loading. Mn-Si-QD was synthesized and evaluated by FT-IR, UV-Vis, fluorescence, SEM, and TEM. The impacts of various factors such as reaction time and reaction temperature were investigated to reach the optimum fluorescence properties. Toxicity on normal and cancerous cells was evaluated with an MTT assay. **Results.** The characterization analysis confirmed successful synthesis, and the MTT assay showed no cytotoxicity on normal cells and showed toxicity on cancerous cells. Magnetopotential showed no difference when compared using OmniScan. In vivo fluorescence imaging was considered and indicated the acceptable (25% ID/g) uptake on the tumor region. The biodistribution study also confirmed the accumulation of the magnetophotoluminescent quantum dot in the tumor site. **Conclusion.** Our research indicated that DOX-loaded Mn-Si-QD is both noninvasive and an agent that can be hopefully used in theranostics.

## 1. Introduction

Breast cancer is a common type of cancer in women and the second cause of cancer death in women aged 45-55 years [1]. While breast cancer is on the rise among women in industrialized countries, it is also on the rise in developing countries [2]. To extend breast cancer survival, reduce the financial burden, and additionally make strides on breast cancer

results, more thought on creating methodologies to determine cancer in the early stages is required [3]. Imaging techniques present more advantages including screening, treatment, and monitoring abilities at any time, do not result in tissue destruction, are minimally invasive procedures, and provide functionality over wide periods and size ranges [4]. Different methods have been developed for breast cancer imaging such as mammography, nuclear medicine,

tomosynthesis, ultrasound, and MRI [5]. Although mammography is the most common screening method, 10-30% of breast cancers can be missed [6]. In contrast, breast MR imaging is the most sensitive technique for detection and stage evaluation. It was understood that MR imaging has higher sensitivity than other imaging techniques especially in high-risk screening (about 77% to 100%). Thus, research on MR imaging agents has delighted scientists. Although the common commercial MRI contrast agent is based on  $Gd^{3+}$ -complexes, research on nonlanthanide metal has attracted attention. Nephrogenic systemic fibrosis (NSF) and  $Gd^{3+}$  deposition in the brain and other organs are serious side effects that worry physicians [7]. Manganese ( $Mn^{2+}$ ), known as a nonlanthanide metal that functions as a  $Gd^{3+}$  alternative, which is essential in cell biology, acts as a nontoxic paramagnetic MRI contrast agent [8]. Compared to  $Gd^{3+}$ ,  $Mn^{2+}$  is a nutritional element that the human body requires and also exhibits all of the physical properties that  $Gd^{3+}$  has [9, 10]. Alhamami et al. claim that in vivo  $Mn^{2+}$ -enhanced MRI was designed to detect early small breast tumors, with the highest sensitivity.  $Mn^{2+}$  describes morphology and tumor borders more obviously than Gd-DTPA [11]. In 2019, Erstad et al. compared the efficacy of Mn-PyC3A to commercial Gd-DOTA and Gd-EOB-DTPA to detect breast cancer and metastatic liver disease in murine models. Results showed that Mn-PyC3A provided comparable tumor contrast enhancement and apparently delayed phase visualization of liver metastases to the  $Gd^{3+}$  agents [12].

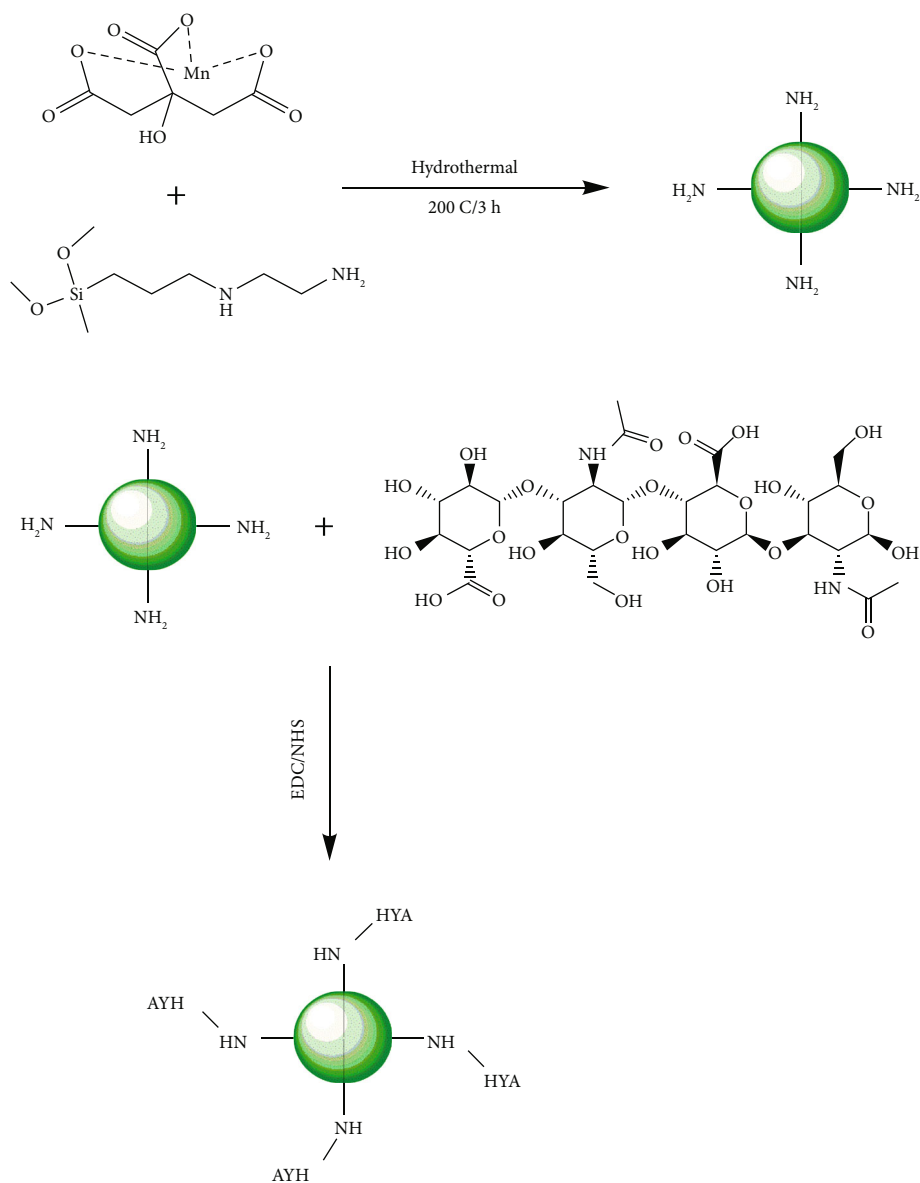
Nanotechnology is a field of science that is based on nanosized materials. It is a novel technology in which particular atomic properties are obtained and has both knowledge and commercial applications [13–15]. Due to the unique features of nanoparticles including having a small size and a high surface-to-volume ratio [16], they are used as a small probe that would allow us to spy on the whole human biological system [17, 18]. Quantum dots (QDs) are nanoscale semiconductor crystals and are nanoparticles that have been used in biological imaging since 1998 [19]. QDs have attracted much attention due to the reduced light scattering and low tissue absorption while most organic dyes do not [20]. Unfortunately, conventional QDs that are made with heavy metals showed a cytotoxic effect [21]. Therefore, for clinical applications, many factors should be considered when designing QDs, including removal of heavy metals [22], use of biodegradable materials that are completely removed from the body [23], use of environmentally safe materials [24], use of materials that are abundant in the earth to which humans have extensive exposure [25], and use of materials that emit near-infrared emission [26]. Silicon quantum dots (Si-QDs) have been considered for their beneficial features such as being abundant in the earth, nontoxic, ecologically safe, and biodegradable and having near-IR emission [26]. In this framework, Erogbogbo et al. designed the highly stable aqueous suspensions of Si-QDs. This biocompatible luminescence was used for pancreatic cancer cell imaging. They highlighted that Si-QDs should be used as a nontoxic optical probe for biomedical diagnostic [27]. One way to improve the imaging performance of this compound is to combine it with other imaging techniques such as MRI. For example, the Erogbogbo group reported

the biocompatible magnetofluorescent nanoprobe. A multimodal nanoprobe that combined Si-QD with iron oxide was used to detect prostate cancer. They stated that Si-QD-based nanocarriers must be expanded to serve as a multimodal platform [28]. Although use of Si-QD-based nanocarriers has been reported in many articles, it is evident that the use of Si-QD-based nanocarriers is still in its infancy. Thus, research on Si-QD-based nanocarriers and its application in medicine is necessary. In most studies, multistep synthesis has been used to synthesize these particles; so far, there are no reports on a one-step synthesis. In this work, for the first time, we introduce the one-step methods for a therapeutic magnetosilicon quantum dot (Mn-Si-QD) agent which combines luminescence with paramagnetic behavior for breast cancer imaging. Also, we studied the ability of this compound for anticancer drug loadings that present a theranostic agent that can overcome the concerns of anticancer and heavy metal toxicity.

## 2. Experimental Methods

*2.1. Characterization Techniques.* All chemical reagents were of analytical grade and used without further purification. Manganese citrate, 2-aminoethyl-3-aminopropyltrimethoxysilane, hyaluronic acid, doxorubicin, EDC, and NHS were purchased from the Sigma-Aldrich Co. (St Louis, MO, USA). Dimethylformamide was purchased from Merck. MCF-7 and HEK-293 cell lines were obtained from the Pasteur Institute (Tehran, Islamic Republic of Iran). Fourier transform infrared spectra (FT-IR) of the powders were acquired using a PerkinElmer Spectrum BX-II spectrometer. The UV-Vis absorption spectra were recorded from 200 to 600 nm using an ultraviolet-visible spectrophotometer by Shimadzu (UV-3101PC; Japan). Both 3D and 2D fluorescence spectroscopy were done using the Nanoimager and FluoVision instruments, respectively. MRI imaging was performed using a Siemens instrument. The surface morphology of the products was investigated using scanning electron microscopy (SEM, LEO-1455VP) and transmission electron microscopy (TEM, JEM-2100). Determination of the quantum yield was performed using quinine sulfate as the control. Excitation and emission of the solution were measured using fluorescence spectroscopy. All studies were repeated three times. The studies were directed in line with the principles of declaration of the Tehran University of Medical Sciences with the following number: IR.TUMS.TIPS.REC.1398.093.

*2.2. Magnetosilicon Quantum Dot Preparation.* Preparation of the Mn-Si-QD is illustrated in Scheme 1. Briefly, manganese citrate (2 mmol) was dissolved in dimethylformamide (12 mL). The solution was then degassed by bubbling nitrogen. Afterwards, 2-aminoethyl-3-aminopropyltrimethoxysilane (3 mL) was added and stirred for 15 min. Then, the solution was autoclaved for 3 hours at 200 degrees centigrade. After cooling the products to room temperature, large particles were separated by centrifuge (10000 rpm, 15 min) and using a dialysis bag (0.5 kDa). Hyaluronic acid (HYA) was conjugated to synthesized nanoparticles by adding 20 mg HYA and 20 mg synthesized nanoparticles in water



SCHEME 1: Preparation path of magnetosilicon quantum dot.

in the presence of EDC/NHS. The mixture was stirred for 24 hours. Finally, the product was purified by centrifuge and using a dialysis bag and then lyophilized.

**2.3. Quantum Yield.** Quantum yield (QY) of the Si-QD was measured using the following method; quinine sulfate (0.05 g quinine sulfate in 270  $\mu\text{L}$   $\text{H}_2\text{SO}_4$  diluted in 5 mL distilled water) was used as the reference. Then, excitation and emission of the prepared solution (1 mL at different concentrations from 0.005 up to 0.01 mg/mL) were measured. Also, 1 mL of the prepared QD with the same concentration of quinine was examined. QY was then calculated using the following equation<sup>34</sup>:

$$\Phi = \Phi' \frac{A' I n^2}{I' A n'^2}, \quad (1)$$

where  $\Phi$  is the QY of the testing sample,  $I$  is the testing sample's integrated emission intensity,  $n$  is the refractive index, and  $A$  is the optical density.  $\Phi'$ ,  $A'$ ,  $I'$ , and  $n'$  are values of the referenced fluorescence dyes of known QYs.

**2.4. Drug Loading and Release.** DOX loading was performed by ultrasonication of 10 mg Mn-Si-QD nanoparticles in 20 mL deionized water for 15 min in 20 degrees centigrade. Then, 4 mg of DOX was dissolved in 2 mL ethanol. The two solutions were mixed together slowly, and the final mixture was stirred for 24 hours at room temperature. Finally, the final product was collected via centrifugation for 15 min and at 8000 rpm. The drug release was performed by dispersing the product in water, and UV-Vis analysis at 480 nm wavelength was conducted via the following equation:

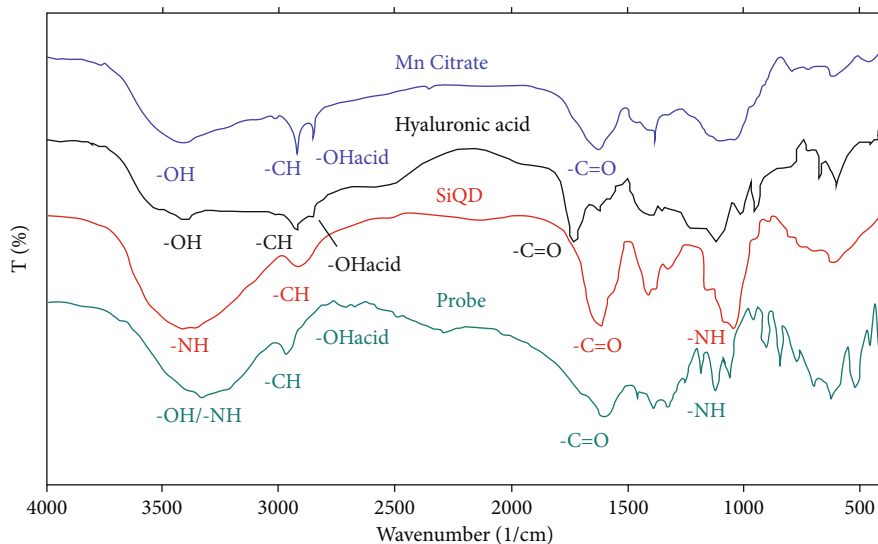


FIGURE 1: FT-IR spectrum of Mn citrate (a), hyaluronic acid (b), Si-QD (c), and Mn-Si-QD (d).

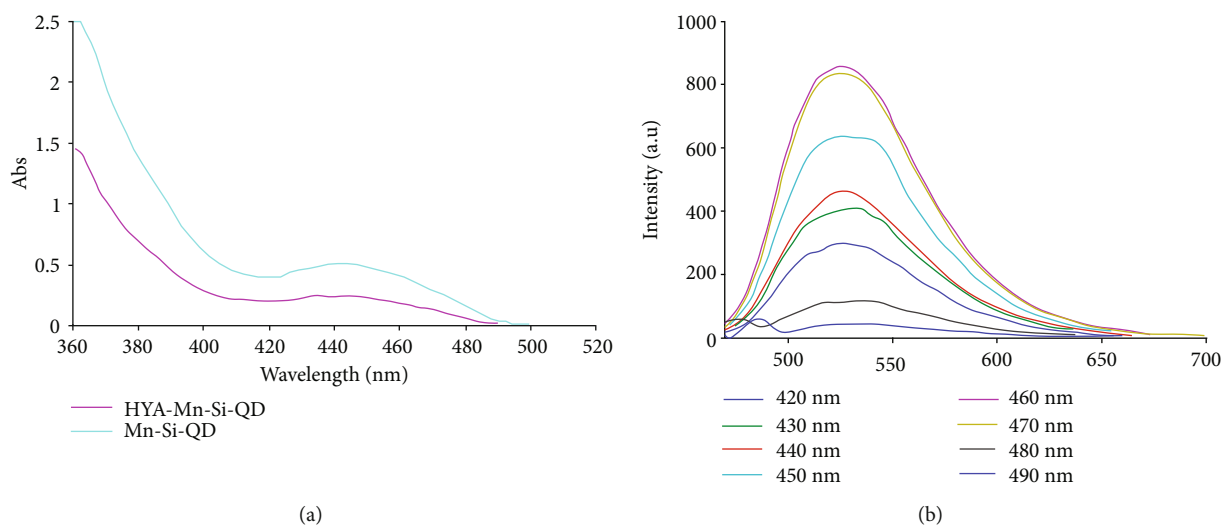


FIGURE 2: (a) UV-Vis spectroscopy of Mn-Si-QD and HYA-Mn-Si-QD and (b) fluorescence spectrum of Mn-Si-QD at different excitation wavelengths.

$$\text{Encapsulation efficiency\%(EE)} = \frac{\text{Total amount of Dox-free Dox in precipitate}}{\text{Total amount of Dox}} * 100,$$

$$\text{Drug loading\%(DL)} = \frac{\text{Total amount of Dox-free Dox in precipitate}}{\text{Mass of final formulation}} * 100.$$

(2)

Drug release was carried out using a dialysis bag (500-1000 kDa) at 37 degrees centigrade and pH = 7.4 and 5.5 at room temperature. Mn-Si-QD-loaded DOX was dissolved in PBS (1:10) and transferred to the dialysis bag. Then, 3 mL of the solution was withdrawn at various times, and 3 mL of PBS was replaced. The release of drug was specified using a UV-Vis spectrophotometer at 359 nm.

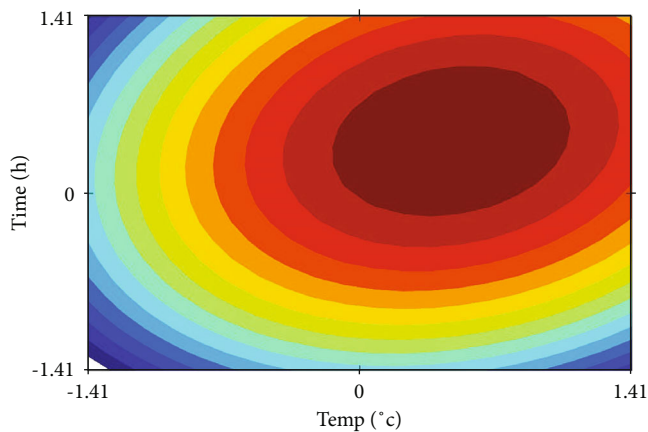


FIGURE 3: Effect of temperature and time on photoluminescence properties.

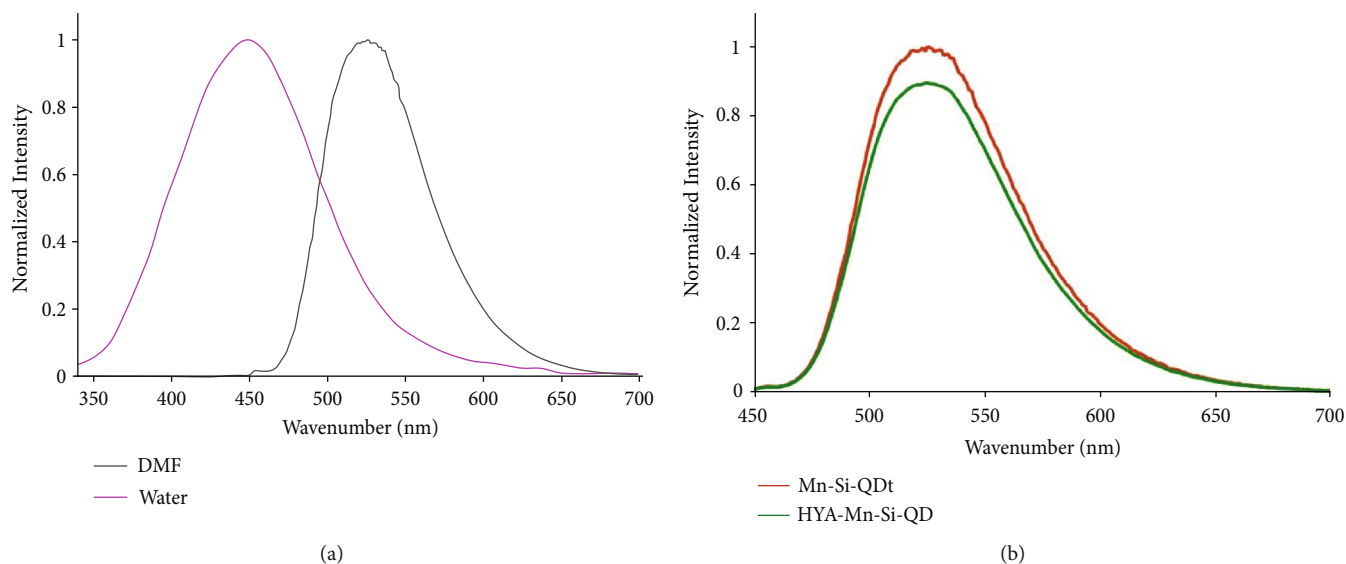


FIGURE 4: (a) Effect of solvent on wavelength and (b) fluorescence spectrum of Mn-Si-QD and HYA-Mn-Si-QD.

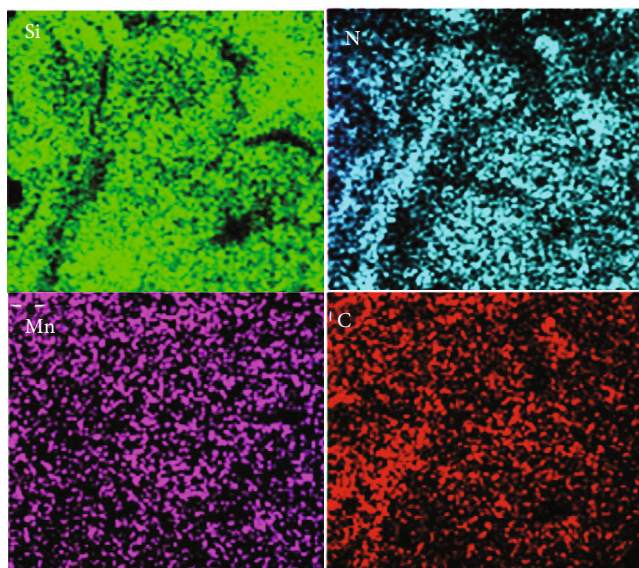


FIGURE 5: Elemental map analysis of Mn-Si-QD.

**2.5. MTT Cytotoxicity Assay.** MTT is a quantitative colorimetric assay for cell viability evaluation. This assay is based on the reduction of tetrazolium (MTT) into insoluble formazan using viable mitochondria. Typically,  $10^4$  cells are suspended in each  $100 \mu\text{L}$  well and incubated at  $37^\circ\text{C}$ . Then,  $20 \mu\text{L}$  of media was withdrawn and  $20 \mu\text{L}$  of prepared solution (5 mg of MTT powder in 1 mL of PBS) was added to each well and incubated for 4 hours. Finally, the media in each well were removed and DMSO was added. Absorption was read at 570 nm using an ELISA reader.

**2.6. MRI Properties.** The Mn-Si-QD solution was prepared in 0.005, 0.01, 0.5, 1, and 2 mg/mL concentrations. For noise attenuation, for each row of product, one row of distilled water was added. MRI images were carried out, and data were analyzed using ImageJ software.

**2.7. In Vivo Fluorescence Imaging and Biodistribution.** For in vivo fluorescence imaging, 3 mice (22 g) were chosen and 0.3 mL of the DOX-loaded Mn-Si-QD was injected. For further investigation, a biodistribution study was performed. The mice were killed, and different organs were harvested and washed with normal saline. Blood was collected via cardiac puncture, and accumulation in each organ was measured. Percentage dose was obtained from the accumulation determined (per gram of tissue) in each organ divided by the total injection.

**2.8. Statistical Analysis.** Statistical analysis was done using SPSS, MATLAB Microsoft Office (2013). For quantitative data analysis, one-way analysis of variance followed by Tukey's test was applied.  $P < 0.05$  was considered statistically significant.

### 3. Result and Discussion

**3.1. Characterization of Mn-Si-QD Nanoparticle.** FT-IR spectrometers were performed to determine the functional groups of the product. The FT-IR spectra of Mn citrate, hyaluronic acid, Si-QD, and Mn-Si-QD are indicated in Figures 1(a)–1(d), respectively. As can be seen in Figures 1(a) and 1(b), the wide and sharp peaks appearing at about  $3500 \text{ cm}^{-1}$  and  $1600 \text{ cm}^{-1}$  belong to the OH group and the carbonyl group of the citrate, respectively. The peak that is located at about  $3000 \text{ cm}^{-1}$  belongs to the CH stretching. In Figure 1(c), the broad peak located at  $3500 \text{ cm}^{-1}$  is associated with the NH group of Si-QD. According to Figure 1(c), CH stretching at around  $3000 \text{ cm}^{-1}$  and the carbonyl band at around  $1600 \text{ cm}^{-1}$  are observed clearly. The sharp peak at about  $1000 \text{ cm}^{-1}$  observed in Figure 1(c) belongs to the Si-O group<sup>35</sup>. The FT-IR spectrum of Mn-Si-QD nanoparticles is shown in Figure 1(d). The extended band around  $3500 \text{ cm}^{-1}$  is related to the OH/NH group. The carbonyl group appears at  $1600 \text{ cm}^{-1}$ . The peaks at  $3000 \text{ cm}^{-1}$  and  $1000 \text{ cm}^{-1}$  are designated as stretched CH

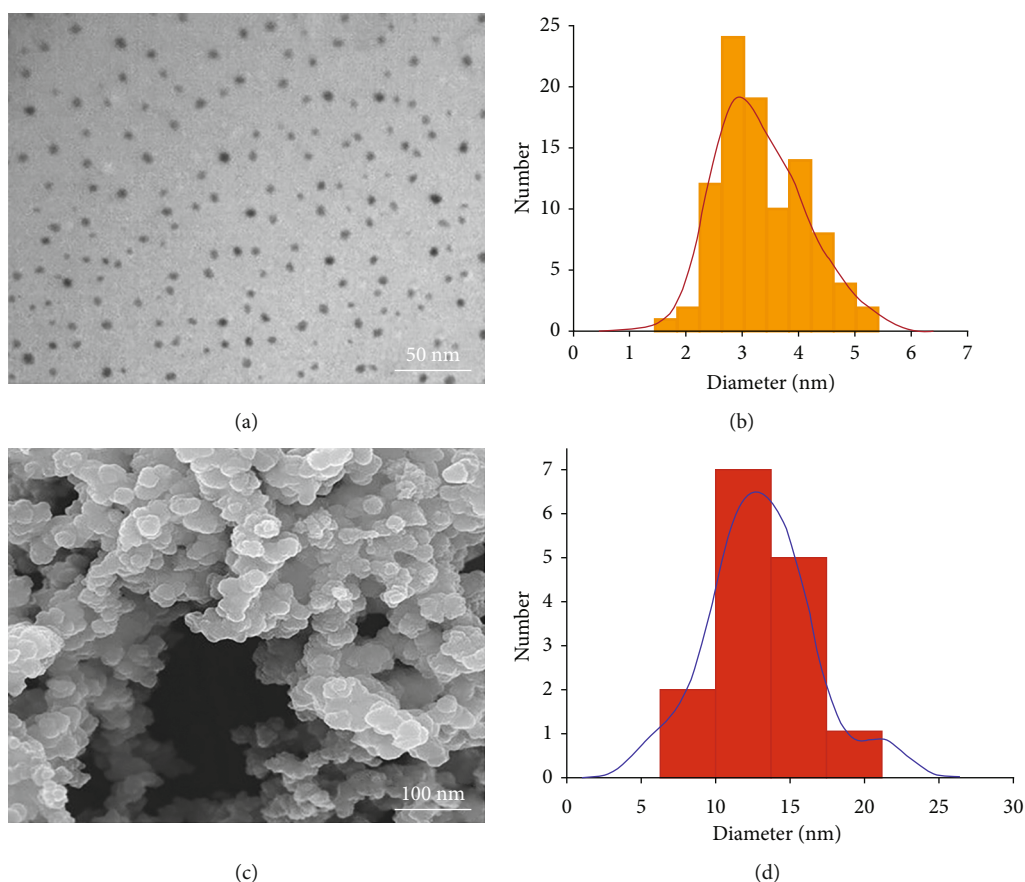


FIGURE 6: (a) TEM and (b) size distribution of Mn-Si-QD and (c) SEM image and (d) size distribution of HYA-Mn-Si-QD (the size distribution obtained from image analysis by ImageJ software).

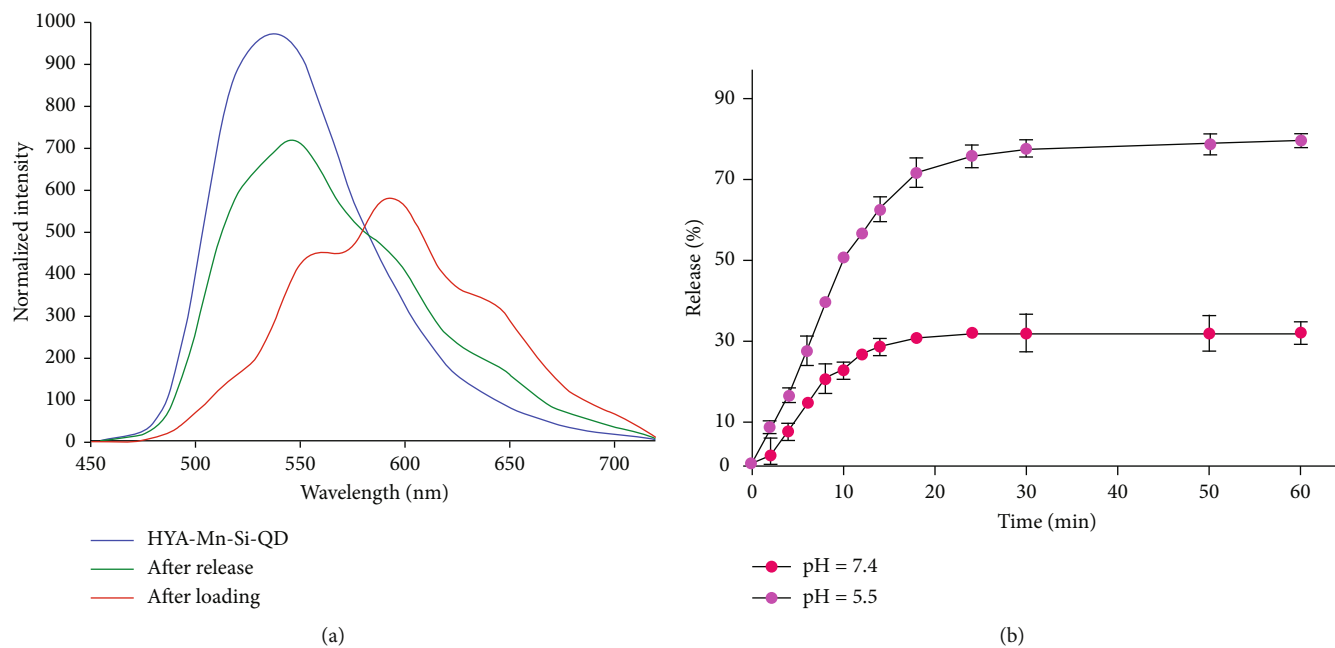


FIGURE 7: (a) Fluorescence spectrum of HYA-Mn-Si-QD of before loading (blue), after loading (red), and after release of DOX (green) and (b) release pattern DOX-loaded Mn-Si-QD in different pH values.

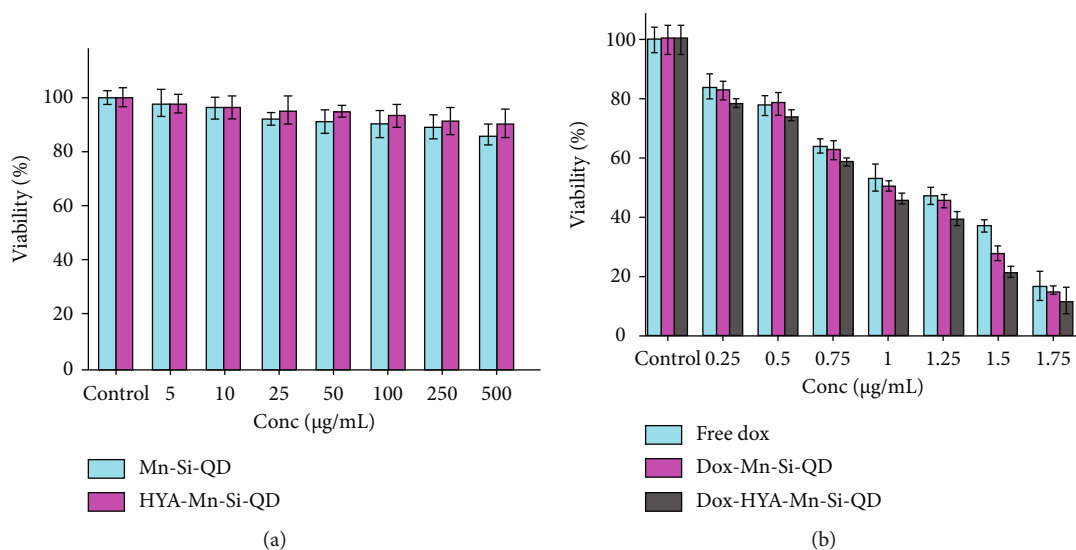


FIGURE 8: MTT assay: HEK-293 cells were exposed to Si-QD and Mn-Si-QD (a) and MCF-7 cells were exposed to free DOX and DOX-loaded Si-QD and Mn-Si-QD (b).

and Si-O functional groups<sup>35</sup>. Therefore, by comparing each spectrum, synthesis and modification of the Mn-Si-QD were confirmed. For further study, UV-Vis spectroscopy of Mn-Si-QD and the conjugation to HYA were analyzed. Figure 2(a) shows the peaks at 360 nm and at about 440 nm which are related to  $\pi - \pi^*$  and  $\pi^* - n$  transitions. In contrast to Mn-Si-QD, HYA conjugated to Mn-Si-QD showed reduced absorption and shifted to the lower wavelength, confirming the covalent bond between Mn-Si-QD and HYA.

**3.2. Excitation-Emission Characterization.** Figure 2(b) shows the emission spectrum at different excitation wavelengths. The maximum emission occurred at 535 nm when excited at 460 nm. QY was determined as 57% using the equation mentioned in Experimental Methods. The effect of temperature and time on photoluminescence properties was considered. The data provided in Figure 3 show that both temperature and time have a direct effect on the emission wavelength. Optimum temperature and time were obtained at 203 degrees centigrade and 3.03 hours, respectively. Furthermore, study on the impact of the solvent indicated that water shifted the wavelength to the shortest and widest which is presented in Figure 4(a). Also, interaction between HYA and Mn-Si-QD had no significant effects on the fluorescence spectrum (Figure 5(b)).

**3.3. Morphological Characteristics.** The elemental mapping analysis was used for determining the elemental composition of the synthesized Mn-Si-QD and quantum dot. The elemental map analysis displays the Mn, N, C, and Si elements (Figure 6). TEM and SEM images were applied to study the detail morphology and size of the samples. The results obtained from the image analysis of the TEM images which show the uniform distribution, spherical morphology, and average diameters of  $3.33 \pm 0.77$  and  $13.03 \pm 3.49$  nm obtained for the quantum dot and HYA-Mn-Si-QD, respectively, are presented in Figure 7.

**3.4. Drug Loading and Release Measurement.** DOX loading in Mn-Si-QD nanoparticle was estimated via the fluorescence spectrum. All experiments are repeated in triplicate. In Figure 7(a), drug loading leads to the formation of the FRET phenomenon by wrapping strategies which can be used as a standard for loading and releasing drugs from nanoparticles [29]. Loading of the drug on the surface of the nanoparticle resulted in an efficiency of 68% for pure Mn-Si-QDs. Due to the fact that the pH of the cancer cell environment is acidic, drug release was evaluated in both neutral and acidic pH. The release profile showed that the largest release of DOX occurred up to the first 30 hours and then became constant. Furthermore, the release pattern depends on the pH of the media. At pH = 7.4, DOX-loaded Mn-Si-QDs showed an approximately 30% release in the first 30 hours and became constant. In contrast, at pH = 5.5, drug release increased up to 70% (Figure 7(b)).

**3.5. Cytotoxicity Assay.** The toxic effect of Si-QD and Mn-Si-QD on the HEK-293 cell lines is demonstrated in Figure 8(a). Data showed that no difference was observed between the treated and control groups up to 500 µg/mL. It means that Si-QD and Mn-Si-QD had no toxic effect on the normal cell line which indicates the biocompatibility of silica quantum dots. This is due to the materials used in the synthesis of this particle. For further investigation, the cytotoxicity of DOX-loaded Mn-Si-QD and HYA-Mn-Si-QD on MCF-7 cell lines was investigated. DOX-loaded HYA-Mn-Si-QD showed a more toxic effect on MCF-7 than free DOX and DOX-loaded Mn-Si-QD which indicates the positive effect of hyaluronic acid in cellular penetration that caused the better treatment (Figure 8(b)). Interestingly, the MTT assay supports our hypothesis that the DOX-loaded HYA-Mn-Si-QD is a theranostic agent. It means that it has both therapy and imaging properties.  $IC_{50}$  values of free DOX, DOX-loaded Si-QDs, and Mn-Si-QDs were 1.103, 1.03, and 0.92, respectively. It can be understood that the

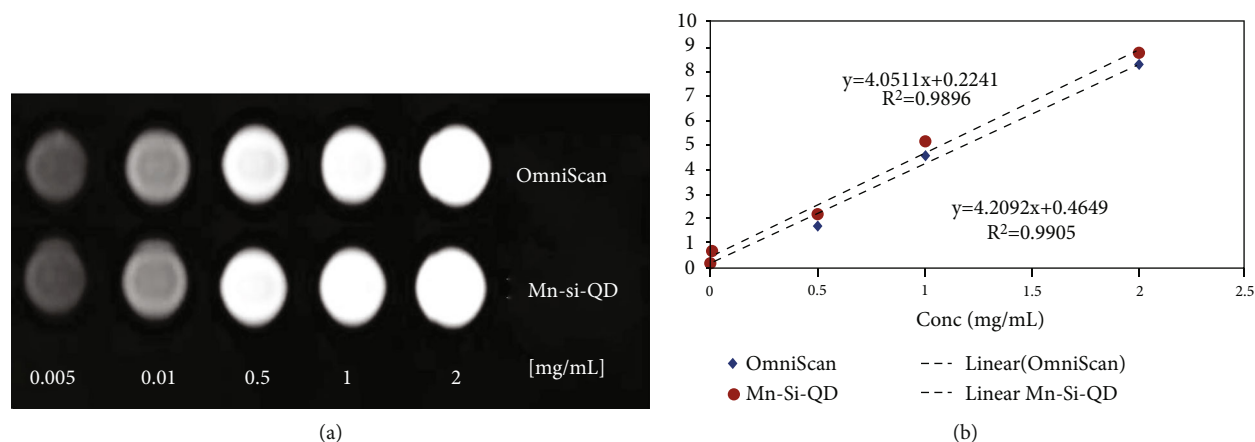


FIGURE 9: Magnetic properties of Mn-Si-QD in contrast to OmniScan.

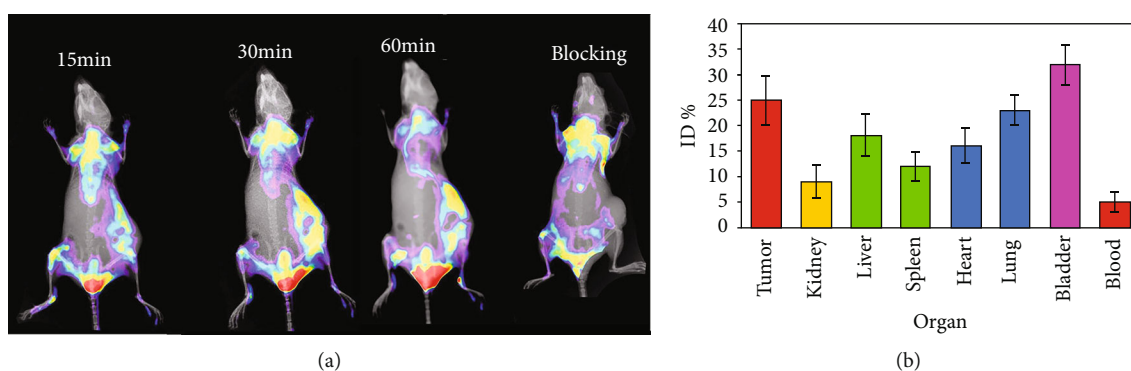


FIGURE 10: (a) In vivo fluorescence imaging of HYA-Mn-Si-QD and (b) biodistribution study of DOX-loaded Mn-Si-QD.

effective dose of DOX-loaded Mn-Si-QDs was less than others. Therefore, the side effect of the drug is reduced due to the reduction of drug dosage.

**3.6. MRI Properties.** For determination of magnetic properties of Mn-Si-QD, an MRI study was done (Figure 9(a)). Data showed that the signal increased by increasing the concentration. Also, Mn-Si-QD was singularly equal compared with OmniScan. In addition, the relaxation time ( $r_1$  was obtained for both Mn-Si-QD and OmniScan)  $4.2 \text{ mL mg}^{-1} \text{ s}^{-1}$  and  $4.06 \text{ mL mg}^{-1} \text{ s}^{-1}$ , respectively) presented in Figure 9(b).

**3.7. Imaging.** In vivo fluorescence imaging was done at 15, 30, and 60 min after injection. According to the in vivo fluorescence image presented in Figure 10(a), the highest accumulation of HYA-Mn-Si-QD was observed 30 minutes after injection. Up until 60 min after injection, appropriate accumulation of the probe was detected in the tumor region. High uptake in the bottom of the mouse body showed the fast excretion of the excess compound. Imaging results were matched with the biodistribution study. The biodistribution study (Figure 10(b)) demonstrated that about 25% of HYA-Mn-Si-QDs was accumulated in the tumor region. Due to the high uptake in the liver and spleen, it can be concluded that the route with the most excretion of HYA-Mn-Si-QDs was through the hepatobiliary system. But urinary system

excretion is also noticeable. High uptake in the lung might be due to the nature of the nanoparticles themselves. Because most of the nanoparticles are suspended, after injection, they aggregate and accumulate in the lung and spleen.

## 4. Conclusion

In this work, for the first time, we synthesized the DOX-loaded magnetophotoluminescent quantum dot. Results showed that the DOX-loaded magnetophotoluminescent quantum dot was successfully synthesized with proper magnetic and photoluminescent properties. Release behavior showed that the largest release was about 70% at  $\text{pH} = 5.5$ . The MTT assay showed no toxicity on normal cells while a toxic effect on cancer cells was obvious. In vivo imaging and biodistribution indicated that the DOX-loaded magnetophotoluminescent quantum dot had a good uptake in the tumor cell. Although the investigation supports our hypothesis that the DOX-loaded magnetophotoluminescent quantum dot can be a theranostic agent, the research is still in its fancy and more studies need to be done.

## Data Availability

All data used to support the findings of this study are included within the article.



## Conflicts of Interest

The authors report no conflict of interest in this work.

## Acknowledgments

The Tehran University of Medical Sciences and Health Services supported this study. The authors wish to thank all the technicians who provided support during the experiments.

## Supplementary Materials

The Supporting Information Results of experimental design. (*Supplementary Materials*)

## References

- [1] M. Ataollahi, J. Sharifi, M. Paknahad, and A. Paknahad, "Breast cancer and associated factors: a review," *Journal of Medicine and Life*, vol. 8, no. Spec Iss 4, pp. 6–11, 2015.
- [2] F. Z. Francies, R. Hull, R. Khanyile, and Z. Dlamini, "Breast cancer in low-middle income countries: abnormality in splicing and lack of targeted treatment options," *American Journal of Cancer Research*, vol. 10, no. 5, pp. 1568–1591, 2020.
- [3] O. Ginsburg, C. H. Yip, A. Brooks et al., "Breast cancer early detection: a phased approach to implementation," *Cancer*, vol. 126, Suppl 10, pp. 2379–2393, 2020.
- [4] A. B. Nover, S. Jagtap, W. Anjum et al., "Modern breast cancer detection: a technological review," *International Journal of Biomedical Imaging*, vol. 2009, Article ID 902326, 2009.
- [5] S. Iranmakani, T. Mortezaadeh, F. Sajadian et al., "A review of various modalities in breast imaging: technical aspects and clinical outcomes," *Egyptian Journal of Radiology and Nuclear Medicine*, vol. 51, no. 1, p. 57, 2020.
- [6] Anonymous, *Changes in cancer detection and false-positive recall in mammography using artificial intelligence: a retrospective, multireader study*, Elsevier BV, 2020.
- [7] S. Deng, R. Ruan, C. K. Mok, G. Huang, X. Lin, and P. Chen, "Inactivation of *Escherichia coli* on almonds using nonthermal plasma," *Journal of Food Science*, vol. 72, no. 2, pp. M62–M66, 2007.
- [8] D. Pan, A. H. Schmieder, S. A. Wickline, and G. M. Lanza, "Manganese-based MRI contrast agents: past, present, and future," *Tetrahedron*, vol. 67, no. 44, pp. 8431–8444, 2011.
- [9] J. Wang, H. Wang, I. A. Ramsay et al., "Manganese-based contrast agents for magnetic resonance imaging of liver tumors: structure–activity relationships and lead candidate evaluation," *Journal of Medicinal Chemistry*, vol. 61, no. 19, pp. 8811–8824, 2018.
- [10] E. M. Gale, I. P. Atanasova, F. Blasi, I. Ay, and P. Caravan, "A manganese alternative to gadolinium for MRI contrast," *Journal of the American Chemical Society*, vol. 137, no. 49, pp. 15548–15557, 2015.
- [11] M. Alhamami, R. B. Mokhtari, T. Ganesh, J. T. Nofiele, H. Yeger, and H.-L. M. Cheng, "Manganese-enhanced magnetic resonance imaging for early detection and characterization of breast cancers," *Molecular Imaging*, vol. 13, no. 7, p. 7290.2014.00021, 2014.
- [12] D. J. Erstad, I. A. Ramsay, V. C. Jordan et al., "Tumor contrast enhancement and whole-body elimination of the manganese-based magnetic resonance imaging contrast agent Mn-PyC3A," *Investigative Radiology*, vol. 54, no. 11, pp. 697–703, 2019.
- [13] S. Bayda, M. Adeel, T. Tuccinardi, M. Cordani, and F. Rizzolio, "The history of nanoscience and nanotechnology: from chemical-physical applications to nanomedicine," *Molecules*, vol. 25, p. 112, 2019.
- [14] M. A. Ebrahimzadeh, S. Mortazavi-Derazkola, and M. A. Zazouli, "Eco-friendly green synthesis of novel magnetic Fe<sub>3</sub>O<sub>4</sub>/SiO<sub>2</sub>/ZnO-Pr<sub>6</sub>O<sub>11</sub> nanocomposites for photocatalytic degradation of organic pollutant," *Journal of Rare Earths*, vol. 38, no. 1, pp. 13–20, 2020.
- [15] M. A. Ebrahimzadeh, A. Naghizadeh, O. Amiri, M. Shirzadi-Ahodashti, and S. Mortazavi-Derazkola, "Green and facile synthesis of Ag nanoparticles using *Crataegus pentagyna* fruit extract (CP-AgNPs) for organic pollution dyes degradation and antibacterial application," *Bioorganic Chemistry*, vol. 94, article 103425, 2020.
- [16] S. Mortazavi-Derazkola, M. A. Ebrahimzadeh, O. Amiri et al., "Facile green synthesis and characterization of *Crataegus microphylla* extract-capped silver nanoparticles ([email protected]) and its potential antibacterial and anticancer activities against AGS and MCF-7 human cancer cells," *Journal of Alloys and Compounds*, vol. 820, article 153186, 2020.
- [17] O. V. Salata, "Applications of nanoparticles in biology and medicine," *Journal of Nanobiotechnology*, vol. 2, no. 1, p. 3-, 2004.
- [18] S. Mortazavi-Derazkola, M. R. Naimi-Jamal, and S. M. Ghor-eishi, "Synthesis, characterization, and atenolol delivery application of functionalized mesoporous hydroxyapatite nanoparticles prepared by microwave-assisted coprecipitation method," *Current Drug Delivery*, vol. 13, no. 7, pp. 1123–1129, 2016.
- [19] C. T. Matea, T. Mocan, F. Tabaran et al., "Quantum dots in imaging, drug delivery and sensor applications," *International Journal of Nanomedicine*, vol. Volume 12, pp. 5421–5431, 2017.
- [20] A. M. Wagner, J. M. Knipe, G. Orive, and N. A. Peppas, "Quantum dots in biomedical applications," *Acta Biomaterialia*, vol. 94, pp. 44–63, 2019.
- [21] S. Hanada, K. Fujioka, Y. Futamura, N. Manabe, A. Hoshino, and K. Yamamoto, "Evaluation of anti-inflammatory drug-conjugated silicon quantum dots: their cytotoxicity and biological effect," *International Journal of Molecular Sciences*, vol. 14, no. 1, pp. 1323–1334, 2013.
- [22] T. Pons, E. Pic, N. Lequeux et al., "Cadmium-free CuInS<sub>2</sub>/ZnS quantum dots for sentinel lymph node imaging with reduced toxicity," *ACS Nano*, vol. 4, no. 5, pp. 2531–2538, 2010.
- [23] J.-H. Park, L. Gu, G. von Maltzahn, E. Ruoslahti, S. N. Bhatia, and M. J. Sailor, "Biodegradable luminescent porous silicon nanoparticles for in vivo applications," *Nature Materials*, vol. 8, no. 4, pp. 331–336, 2009.
- [24] V. L. Colvin, "The potential environmental impact of engineered nanomaterials," *Nature Biotechnology*, vol. 21, no. 10, pp. 1166–1170, 2003.
- [25] G. Plumlee, S. Morman, and T. Ziegler, "The toxicological geochemistry of earth materials: an overview of processes and the interdisciplinary methods used to understand them," *Reviews in Mineralogy and Geochemistry*, vol. 64, no. 1, pp. 5–57, 2006.
- [26] W. Cai, D. W. Shin, K. Chen et al., "Peptide-labeled near-infrared quantum dots for imaging tumor vasculature in living subjects," *Nano Letters*, vol. 6, no. 4, pp. 669–676, 2006.

- [27] F. Erogbogbo, K.-T. Yong, I. Roy, G. Xu, P. N. Prasad, and M. T. Swihart, "Biocompatible luminescent silicon quantum dots for imaging of cancer cells," *ACS Nano*, vol. 2, no. 5, pp. 873–878, 2008.
- [28] F. Erogbogbo, K.-T. Yong, R. Hu et al., "Biocompatible magnetofluorescent probes: luminescent silicon quantum dots coupled with superparamagnetic iron (III) oxide," *ACS Nano*, vol. 4, no. 9, pp. 5131–5138, 2010.
- [29] N. T. Chen, S. H. Cheng, C. P. Liu et al., "Recent advances in nanoparticle-based Förster resonance energy transfer for biosensing, molecular imaging and drug release profiling," *International Journal of Molecular Sciences*, vol. 13, no. 12, pp. 16598–16623, 2012.